INSTITUTE OF PHYSICS PUBLISHING INVERSE PROBLEMS

Inverse Problems **18** (2002) L11–L19 PII: S0266-5611(02)39995-7

LETTER TO THE EDITOR

On single-photon emission computed tomography imaging based on an exact formula for the nonuniform attenuation correction

J-P Guillement[1], **F Jauberteau**[1], **L Kunyansky**[2], **R Novikov**[1] **and R Trebossen**[3]

[1] CNRS, UMR 6629, Département de Mathématiques, Université de Nantes, BP 92208, F-44322, Nantes Cedex 03, France
[2] Department of Mathematics, University of Arizona, N Santa Rita 617, Tucson, AZ 85721, USA
[3] Service Hospitalier Frédéric Joliot, CEA, 4 place du General Leclerc, 91401 Orsay Cedex, France

E-mail: guillement@math.univ-nantes.fr, jauberteau@math.univ-nantes.fr, leonk@math.arizona.edu, novikov@math.univ-nantes.fr and trebosse@shfj.cea.fr

Received 26 July 2002
Published 10 October 2002
Online at stacks.iop.org/IP/18/L11

Abstract
We develop an exact formula approach to nonuniform attenuation correction in single-photon emission computed tomography (SPECT). We discuss several reconstruction examples obtained by this method from real SPECT data.

1. Introduction

We consider the two-dimensional attenuated x-ray transformation P_a defined by the formula

$$P_a f(s,\theta) = \int_{\mathbb{R}} \exp(-Da(s\theta^\perp + t\theta, \theta))\, f(s\theta^\perp + t\theta)\, \mathrm{d}t, \qquad (s,\theta) \in \mathbb{R}\times\mathbb{S}^1, \quad \theta^\perp = (-\theta_2, \theta_1) \quad \text{for } \theta = (\theta_1,\theta_2) \in \mathbb{S}^1, \tag{1.1a}$$

$$Da(x,\theta) = \int_0^{+\infty} a(x + t\theta)\, \mathrm{d}t, \qquad (x,\theta) \in \mathbb{R}^2 \times \mathbb{S}^1, \tag{1.1b}$$

where a and f are real-valued, sufficiently regular functions on $\mathbb{R}^2$ sufficiently rapidly vanishing at infinity, a is a parameter (attenuation coefficient), Da is the divergent beam transform of a, f is a test function. In addition, we interpret $\mathbb{R}\times\mathbb{S}^1$ as the set of all oriented straight lines in $\mathbb{R}^2$. If $\gamma = (s,\theta) \in \mathbb{R}\times\mathbb{S}^1$ then $\gamma = \{x \in \mathbb{R}^2 | x = s\theta^\perp + t\theta, t \in \mathbb{R}\}$ (modulo orientation) and θ gives the orientation of γ.

The transformation P_a and the problem of its inversion (under the condition that a is known) arise in single-photon emission computed tomography (SPECT); see, for example, [Na1]. In SPECT (as soon as the problem is restricted to a fixed two-dimensional plane Ξ

identified with $\mathbb{R}^2$), f is the density of emitters of x-rays (the radionuclide distribution), a is the linear x-ray attenuation coefficient of the medium, and $P_a f(\gamma)$, $\gamma = (s, \theta) \in \mathbb{R} \times \mathbb{S}^1$, is (approximately) the measured emission intensity in the direction θ at a detector at '$+\infty$' on γ (at a detector on the connected component of $\gamma \setminus (\operatorname{supp} f \cup \operatorname{supp} a)$ containing $+\infty$ on γ).

We consider the following inversion formula for the transformation P_a:

$$f(x) = \frac{1}{4\pi}\left(-\frac{\partial}{\partial x_1}\int_{\mathbb{S}^1} K(x,\theta)\theta_2 \,\mathrm{d}\theta + \frac{\partial}{\partial x_2}\int_{\mathbb{S}^1} K(x,\theta)\theta_1 \,\mathrm{d}\theta\right), \tag{1.2a}$$

$$K(x,\theta) = \exp(Da(x,\theta) - A_\theta(x\theta^\perp))h_\theta(x\theta^\perp), \tag{1.2b}$$

$$h_\theta(s) = \cos(B_\theta(s))H(\exp(A_\theta)\cos(B_\theta)g_\theta)(s) + \sin(B_\theta(s))H(\exp(A_\theta)\sin(B_\theta)g_\theta)(s), \tag{1.2c}$$

$$A_\theta(s) = \tfrac{1}{2}Pa(s,\theta), \qquad B_\theta(s) = HA_\theta(s), \qquad g_\theta(s) = P_a f(s,\theta), \tag{1.2d}$$

where $P = P_0$ is the classical two-dimensional x-ray transformation, H is the Hilbert transformation defined by the formula

$$Hu(s) = \frac{1}{\pi} pv \int_{\mathbb{R}} \frac{u(t)}{s-t}\,\mathrm{d}t, \tag{1.3}$$

where u is a test function, $x = (x_1, x_2) \in \mathbb{R}^2$, $\theta = (\theta_1, \theta_2) \in \mathbb{S}^1$, $\theta^\perp = (-\theta_2, \theta_1)$, $s \in \mathbb{R}$, $\mathrm{d}\theta$ is the standard element of arc length on $\mathbb{S}^1$.

In a slightly different form (using complex notations) the formula (1.2) was obtained in [No1]. The formula (1.2) was successfully implemented numerically in [Ku] and in [Na2].

In the present note we give the first application of the formula (1.2) to the attenuation correction in real SPECT imaging, i.e. to finding a real radionuclide distribution f on $\mathbb{R}^2$ from real SPECT projections $g \approx P_a f$ on $\mathbb{R} \times \mathbb{S}^1$, under the condition that a on $\mathbb{R}^2$ is approximately known (and $a \not\approx 0$). Note that in SPECT one finds a in advance by methods of transmission computed tomography.

In section 2 we discuss the SPECT reconstruction algorithm based on (1.2) and in section 3 we give examples of reconstruction from real SPECT data provided by the Service Hospitalier Frédéric Joliot.

Concerning other results given in the literature on the attenuation correction problem in SPECT, see references given in [Na1, MIMIKIH, Ku, No2]. In particular, the reader interested in the history of analytic inversion methods and formulae in SPECT is referred to [Ku, No1, No2].

2. Reconstruction algorithm

The formula (1.2) admits a numerical implementation via a direct generalization of the filtered backprojection (FBP) algorithm (see [Na1] for the description of the FBP algorithm). This implementation follows the obvious structure of (1.2) and takes H with low-frequency filters (where a low-frequency filter for H in (1.2d) can differ from a low-frequency filter for H in (1.2c)). Note that H with a low-frequency filter $\hat{w}$ can be viewed as the transformation H_w defined by the formula

$$\begin{aligned} H_w u(s) &= \frac{1}{\sqrt{2\pi}}\int_{\mathbb{R}} \mathrm{e}^{\mathrm{i}s\sigma}\hat{w}(\sigma)\frac{\operatorname{sgn}(\sigma)}{\mathrm{i}}\hat{u}(\sigma)\,\mathrm{d}\sigma, \\ \hat{u}(\sigma) &= \frac{1}{\sqrt{2\pi}}\int_{\mathbb{R}} \mathrm{e}^{-\mathrm{i}s\sigma}u(s)\,\mathrm{d}s, \end{aligned} \tag{2.1}$$

where u is a test function, $\hat{w}(\sigma) \sim 1$ for small $|\sigma|$ and $\hat{w}(\sigma) \sim 0$ for large $|\sigma|$.

The above-mentioned SPECT reconstruction algorithm based on (1.2) was proposed and successfully implemented numerically in [Ku]. A similar algorithm was also developed in [Na2].

The work [Ku] contains a detailed description of the algorithm and gives a variety of numerical examples showing that the algorithm is capable of accurately finding f from $g \approx P_a f$ and a even in the case of a strongly nonuniform attenuation coefficient a and moderately noisy projections g. Nevertheless, numerical examples of [Ku] also showed that the algorithm of [Ku] is more sensitive to noise in projections than the FBP algorithm and, therefore, to apply (1.2) to real SPECT imaging, further investigations are necessary. In addition, some approaches increasing the stability of the algorithm of [Ku] are discussed in the preprint version of [Ku].

In the following part of this section we describe the scheme we use to apply (1.2) to real SPECT imaging.

We decompose f and K of (1.2) as follows:

$$f(x) = \varepsilon_1(x) + \varepsilon_2(x), \tag{2.2a}$$

$$K(x,\theta) = K_1(x,\theta) + K_2(x,\theta), \tag{2.2b}$$

$$\varepsilon_j(x) = \frac{1}{4\pi}\left(-\frac{\partial}{\partial x_1}\int_{\mathbb{S}^1} K_j(x,\theta)\theta_2\,\mathrm{d}\theta + \frac{\partial}{\partial x_2}\int_{\mathbb{S}^1} K_j(x,\theta)\theta_1\,\mathrm{d}\theta\right), \qquad j = 1,2, \tag{2.2c}$$

$$\begin{aligned} &K_1(x,\theta) = h_\theta(x\theta^\perp),\\ &K_2(x,\theta) = (\exp(Da(x,\theta) - A_\theta(x\theta^\perp)) - 1)h_\theta(x\theta^\perp), \end{aligned} \tag{2.2d}$$

where $x \in \mathbb{R}^2, \theta \in \mathbb{S}^1, h$ is defined by (1.2c). The function ε_1 computed via (2.2c), (2.2d), (1.2c), (1.2d) on the basis of the algorithm of [Ku] is considerably less sensitive to noise in projections g than the function ε_2 computed similarly. Therefore, for the case of considerably noisy projections g, when computing K_1 we filter g in one way and when computing K_2 we filter g in another (stronger) way.

Given SPECT projections g and the attenuation distribution a, we consider:

(I)

$$g^-_\theta(s) = \begin{cases} g_\theta(s) - c_\theta(s) & \text{for } g_\theta(s) - c_\theta(s) \geqslant 0\\ 0 & \text{for } g_\theta(s) - c_\theta(s) < 0, \end{cases} \tag{2.3}$$

where $(s,\theta) \in \mathbb{R}\times\mathbb{S}^1$, $c_\theta(s)$ is a non-negative function approximating the average noise of photon scattering. In the simplest nonzero approximation (actually used in the present work) $c_\theta(s)$ is identically the constant equal to the average intensity measured by detectors along oriented straight lines passing near the object (containing emitters of x-rays) but not intersecting it;

(II)

$$\begin{aligned} &\eta_j g^-_{\theta(\varphi)}(s) = \frac{1}{2\pi}\int_{\mathbb{R}}\sum_{k\in\mathbb{Z}} \hat\eta_j(\sigma,k)\hat g^-(\sigma,k)\mathrm{e}^{\mathrm{i}k\varphi}\mathrm{e}^{\mathrm{i}s\sigma}\,\mathrm{d}\sigma, \qquad j = 1,2,\\ &\hat g^-(\sigma,k) = \frac{1}{2\pi}\int_{\mathbb{R}}\int_0^{2\pi} g^-_{\theta(\varphi)}(s)\mathrm{e}^{-\mathrm{i}k\varphi}\mathrm{e}^{-\mathrm{i}s\sigma}\,\mathrm{d}\varphi\,\mathrm{d}s, \end{aligned} \tag{2.4}$$

where $s \in \mathbb{R}, \varphi \in [0,2\pi], \theta(\varphi) = (\cos\varphi, \sin\varphi), \sigma \in \mathbb{R}, k \in \mathbb{Z}$, $\hat\eta_1, \hat\eta_2$ are two-dimensional low-frequency filters;

(III)

$$\begin{aligned} &\tilde a(x) = \chi_1 a(x) = \frac{1}{2\pi}\int_{\mathbb{R}^2}\hat\chi_1(p)\hat a(p)\mathrm{e}^{\mathrm{i}px}\,\mathrm{d}p, \qquad x \in \mathbb{R}^2,\\ &\hat a(p) = \frac{1}{2\pi}\int_{\mathbb{R}^2} a(x)\mathrm{e}^{-\mathrm{i}px}\,\mathrm{d}x, \qquad p \in \mathbb{R}^2, \end{aligned} \tag{2.5}$$

where $\hat{\chi}_1$ is a two-dimensional low-frequency filter;

(IV)

$$f_1(x) = \chi_2 f(x) = \frac{1}{2\pi}\int_{\mathbb{R}^2} \hat{\chi}_2(p)\hat{f}(p)\mathrm{e}^{\mathrm{i}px}\,\mathrm{d}p, \qquad x \in \mathbb{R}^2,$$
$$\hat{f}(p) = \frac{1}{2\pi}\int_{\mathbb{R}^2} f(x)\mathrm{e}^{-\mathrm{i}px}\,\mathrm{d}x, \qquad p \in \mathbb{R}^2, \tag{2.6}$$

where f is constructed via (1.2a), (2.2b), (2.2d), (1.2c), (1.2d) (on the basis of the above-mentioned algorithm of [Ku]), where a is replaced by $\tilde{a} = \chi_1 a$, g is replaced by $\eta_1 g^-$ and $\eta_2 g^-$ in, respectively, the computations for K_1 and K_2, and $\hat{\chi}_2$ is a two-dimensional low-frequency filter.

We consider f_1 of (2.6) as the first approximation to the real radionuclide distribution f^{real}. The use of the low-frequency filters $\hat{\eta}_1$, $\hat{\eta}_2$, $\hat{\chi}_1$, $\hat{\chi}_2$ permits us to increase considerably the stability of the initial algorithm of [Ku]. The use of the filter $\hat{\chi}_1$ also permits us to make an additional correction on photon scattering. As soon as f_1 is found we consider

$$\lambda_1 = \frac{\|P_{\tilde{a}} f_1 - g^-\|}{\|g^-\|}, \tag{2.7}$$

where the norm $\|\cdot\|$ is defined by the formula

$$\|u\| = \tfrac{1}{2}\left(\int_{\mathbb{S}^1}\int_{\mathbb{R}} (1+\exp[P\tilde{a}(s,\theta)])^2 |u(s,\theta)|^2\,\mathrm{d}s\,\mathrm{d}\theta\right)^{1/2}. \tag{2.8}$$

We say that f_1 is a good approximation to the real radionuclide distribution f^{real} if λ_1 is considerably smaller than 1. To improve the reconstruction result given by f_1, we proceed as follows. We compute

$$G_\theta(s) = (g^-_\theta(s)+\mu)\frac{Pf_1(s,\theta)+\mu}{P_{\tilde{a}} f_1(s,\theta)+\mu} - \mu, \qquad (s,\theta) \in \mathbb{R}\times\mathbb{S}^1, \tag{2.9}$$

where μ is some sufficiently small positive constant depending on $P_{\tilde{a}} f_1$ such that $P_{\tilde{a}} f_1(s,\theta)+\mu > 0$ for $(s,\theta) \in \mathbb{R}\times\mathbb{S}^1$. We consider G as an approximation to the unattenuated x-ray transform Pf^{real} of the real radionuclide distribution f^{real}. We enforce the conditions

$$g^-_\theta(s) \leqslant G_\theta(s) \leqslant \exp(P\tilde{a}(s,\theta))g^-_\theta(s), \qquad (s,\theta) \in \mathbb{R}\times\mathbb{S}^1, \tag{2.10}$$

and compute

$$f_2 = P^{-1}G \tag{2.11}$$

using (1.2) with $a \equiv 0$ and H_w (defined by (2.1)) in place of H (i.e. using a variant of the classical FBP algorithm). We consider f_2 as the second approximation to the real radionuclide distribution f^{real}.

Note that the passage from f_1 to f_2 via (2.9)–(2.11) is a variation of the step of the iterative SPECT reconstruction algorithm of [MNOY] (see also a review of [MIMIKIH]) and is a variation of the techniques proposed in section 6.2 of the preprint version of [Ku] to increase the stability of the initial algorithm based on (1.2).

As soon as f_2 is found we consider

$$\lambda_2 = \frac{\|P_{\tilde{a}} f_2 - g^-\|}{\|P_{\tilde{a}} f_1 - g^-\|}, \tag{2.12}$$

where the norm is defined by (2.8). We say that f_2 gives a better reconstruction result than f_1 if λ_2 is noticeably smaller than 1.

Note that if λ_2 is considerably smaller than 1 we continue the iterative reconstruction with the step described by (2.9)–(2.11) as long as the reconstruction result considerably improves.

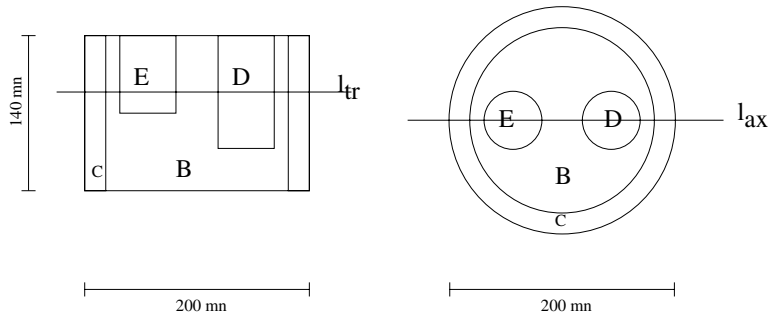

Figure 1. Axial (left) and transverse (right) sections through the phantom. The position of the lines l_{tr}, l_{ax} indicate the level of the section on the alternate image.

3. Reconstruction examples

We consider a version of the so-called Utah phantom (designed at the 2nd International Meeting on fully Three-Dimensional Image Reconstruction in Radiology and Nuclear Medicine, Snowbird, Utah, 1993). The geometry of the phantom is shown in figure 1. Geometrically, the phantom consists of a large cylinder (B) surrounded by an annulus (C) and of two cylinders (D) and (E) inserted in the large cylinder. In addition: C= 20 mm (annular width), D= 43 mm (diameter) $\times$ 105 mm (length), E = 43 mm (diameter) $\times$ 55 mm (length).

In our experiment, the regions (E) and (D) were filled with solutions (NH_4I and K_2HPO_4, respectively) of high density but without any activity for the emission acquisition, the regions (B) and (C) were filled with water and with a radioactive solution (I^{123}) of 763 and 772 nl ml^{-1}, respectively.

In the present note we deal with SPECT imaging for three different transverse sections through the phantom. We consider the transverse sections by planes Ξ_1, Ξ_2, Ξ_3, where Ξ_1 intersects only (B) and (C), Ξ_2 intersects only (B), (C) and (D), Ξ_3 intersects (B), (C), (D) and (E). The section by Ξ_3 coincides with the transverse section of figure 1.

For each of our examples of SPECT imaging, the data (we reconstructed from) consist of an attenuation map and emission data. The attenuation map was obtained using the transmission tomography and consists of approximate values of the attenuation coefficient on a 129 $\times$ 129 grid with pixel size 3.4 mm. The emission data consist of 128 projections equispaced in 360° with 129 samples (and the discretization step 3.4 mm) each. We compute the image on the same 129 $\times$ 129 grid on which the attenuation map is given.

Figures 2(A)–(C) show the attenuation maps on the planes Ξ_1, Ξ_2, Ξ_3, respectively. Figures 3(A)–(C) show the profiles (with their maximum values) of the attenuation maps 2(A)–(C), respectively, at the level of the axial section through the phantom. Figures 4(A)–(C) show the emission data for the sections by Ξ_1, Ξ_2, Ξ_3, respectively. Note that the emission data were measured with the energy window $0.9E$–$1.1E$, where E = 159 keV is the major energy peak of I^{123}, at 60 s/projection, the radius of rotation was 261 mm. Our main reconstruction results on Ξ_1, Ξ_2, Ξ_3 are shown in figures 5–8.

Notice that all two-dimensional images of the present work were drawn using a linear grey scale, in such a way that the dark grey colour represents zero (or negative values, if any) and white corresponds to the maximum value of the imaged function.

Images shown in figures 5(A), 6(A), 7(A) were obtained as the first approximation f_1 of section 2 (see (2.6)). In addition, the low-frequency filters $\hat{\eta}_1$, $\hat{\eta}_2$, $\hat{\chi}_1$, $\hat{\chi}_2$, were taken as

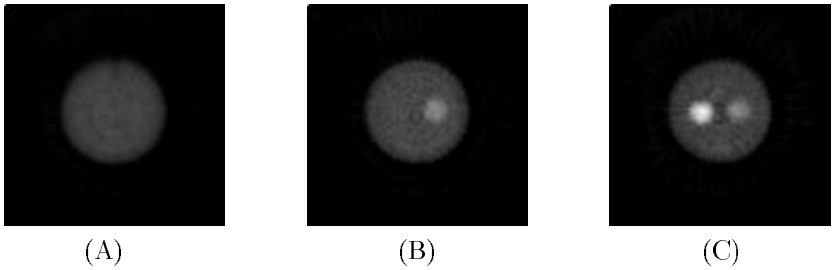

Figure 2. Attenuation maps on Ξ_1, Ξ_2, Ξ_3.

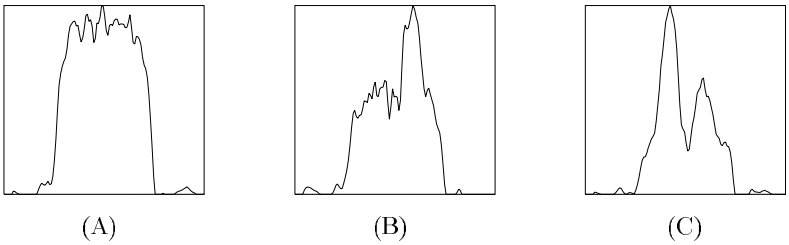

Figure 3. Profiles (with their maximum values) of the images 2(A)–(C) at the level of the axial section through the phantom: (A) max $= 0.1$ cm^{-1}, (B) max $= 0.24$ cm^{-1}, (C) max $= 0.4$ cm^{-1}.

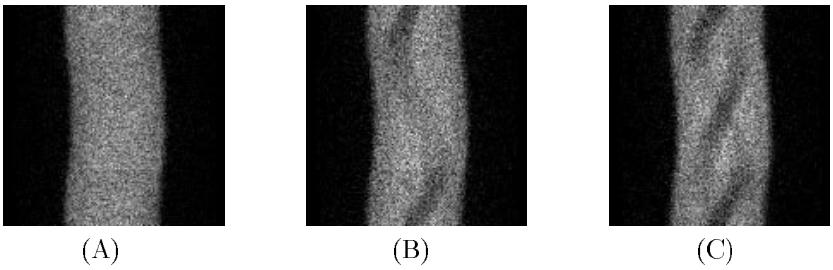

Figure 4. Emission data $g_{(\cos\varphi,\sin\varphi)}(s)$ for the sections by Ξ_1, Ξ_2, Ξ_3. (For each of figures (A)–(C) the angle φ increases from 0 at the bottom to 2π at the top and s increases from right to left.)

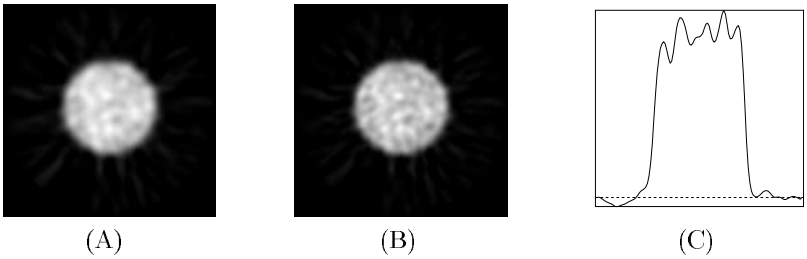

Figure 5. Stabilized reconstruction on Ξ_1 (for $\alpha_1 = 1/2, \alpha_2 = 1/3, \beta = 1/2$). (A) First approximation with $\lambda_1 = 0.17$. (B) Second approximation with $\lambda_2 = 0.97$. (C) Profile of the image B at the level of the axial section through the phantom.

follows:

$$\hat{\eta}_1(\sigma,k) = \begin{cases} \left(\dfrac{\sin(\pi\sigma/\alpha_1\sigma_{nyq})}{\pi\sigma/\alpha_1\sigma_{nyq}}\right)^2 & \text{for } |\sigma| \leqslant \alpha_1\sigma_{nyq}, \\ 0 & \text{for } |\sigma| > \alpha_1\sigma_{nyq} \end{cases} \tag{3.1}$$

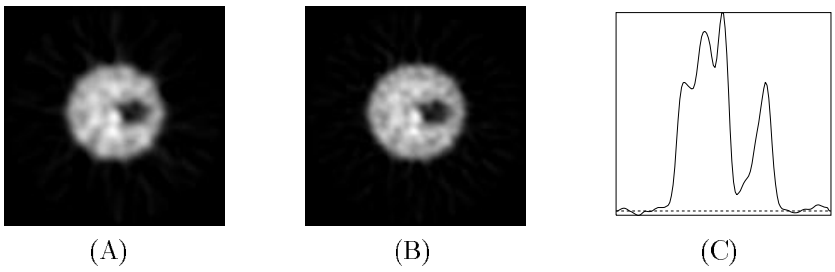

Figure 6. Stabilized reconstruction on Ξ_2 (for $\alpha_1 = 1/2, \alpha_2 = 1/3, \beta = 1/2$). (A) First approximation with $\lambda_1 = 0.21$. (B) Second approximation with $\lambda_2 = 0.94$. (C) Profile of the image B at the level of the axial section through the phantom.

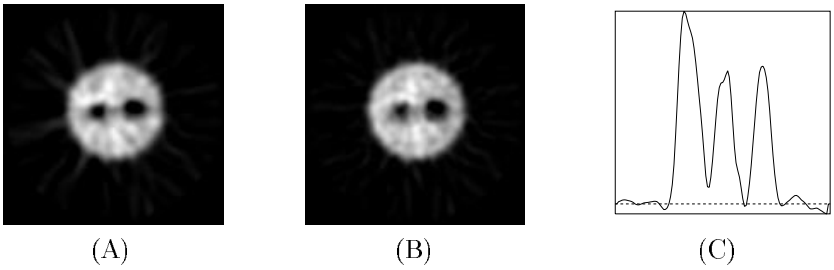

Figure 7. Stabilized reconstruction on Ξ_3 (for $\alpha_1 = 1/2, \alpha_2 = 1/3, \beta = 1/2$). (A) First approximation with $\lambda_1 = 0.24$. (B) Second approximation with $\lambda_2 = 0.87$. (C) Profile of the image B at the level of the axial section through the phantom.

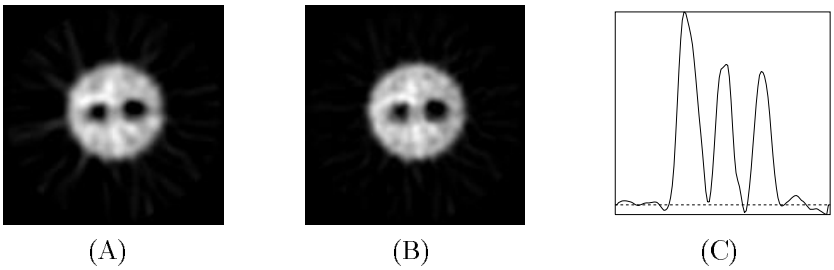

Figure 8. Stabilized reconstruction on Ξ_3 (for $\alpha_1 = 1/2, \alpha_2 = 1/3, \beta = 1/4$). (A) First approximation with $\lambda_1 = 0.23$. (B) Second approximation with $\lambda_2 = 0.89$. (C) Profile of the image B at the level of the axial section through the phantom.

$$\hat{\eta}_2(\sigma,k) = \begin{cases} \left(\dfrac{\sin(\pi\sigma/\alpha_2\sigma_{nyq})}{(\pi\sigma/\alpha_2\sigma_{nyq})}\dfrac{\sin(\pi k/\alpha_2 k_{nyq})}{(\pi k/\alpha_2 k_{nyq})}\right)^2 & \text{for } |\sigma| \leqslant \alpha_2\sigma_{nyq},\ |k| \leqslant \alpha_2 k_{nyq}, \\ 0 & \text{for } |\sigma| > \alpha_2\sigma_{nyq} \text{ or } |k| \geqslant \alpha_2 k_{nyq}, \end{cases} \tag{3.2}$$

where σ_{nyq}, k_{nyq} denote the Nyquist frequencies of the discretization in s, φ, respectively, and α_1, α_2 were taken as $1/2$, $1/3$, respectively;

$$\hat{\chi}_1(p) = \begin{cases} \left(\dfrac{\sin(\pi|p|/\beta\omega)}{\pi|p|/\beta\omega}\right)^2 & \text{for } |p| \leqslant \beta\omega, \\ 0 & \text{for } |p| > \beta\omega, \end{cases} \tag{3.3}$$

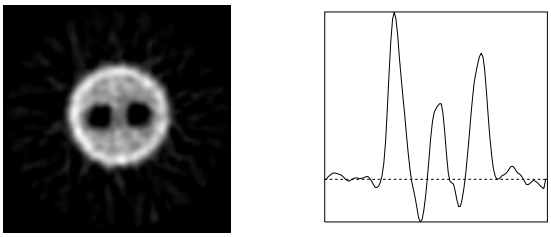

(A) (B)

Figure 9. Regularized reconstruction on Ξ_3 with no attenuation correction; the two-dimensional image (left) and its profile at the level of the axial section through the phantom (right).

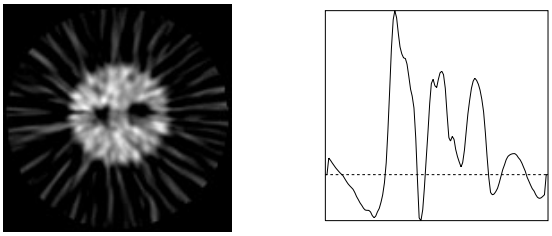

(A) (B)

Figure 10. Regularized reconstruction on Ξ_3 by the initial algorithm of [Ku] (with no filters $\hat{\eta}_1, \hat{\eta}_2, \hat{\chi}_1, \hat{\chi}_2$); the two-dimensional image (left) and its profile at the level of the axial section through the phantom (right).

$$\hat{\chi}_3(p) \equiv 1, \tag{3.4}$$

where ω denotes the Nyquist frequency of the discretization in x and β was taken as $1/2$. In addition, the Hilbert transformation H in (1.2c), (1.2d) was taken with the low-frequency filters $\hat{w}_1$, $\hat{w}_2$, respectively, as follows:

$$\hat{w}_1(\sigma) = \begin{cases} \left(\dfrac{\sin(\pi\sigma/\alpha_1\sigma_{nyq})}{\pi\sigma/\alpha_1\sigma_{nyq}}\right)^2 & \text{for } |\sigma| \leqslant \alpha_1\sigma_{nyq}, \\ 0 & \text{for } |\sigma| > \alpha_1\sigma_{nyq}, \end{cases} \tag{3.5}$$

$$\hat{w}_2(\sigma) = \frac{\sin(\pi\sigma/\sigma_{nyq})}{\pi\sigma/\sigma_{nyq}}, \tag{3.6}$$

where σ_{nyq} and α_1 are as in (3.1).

Images shown in figures 5(B), 6(B), 7(B) were obtained as the second approximation f_2 of section 2 (see (2.11)). In addition, the Hilbert transformation H in (1.2) with $a \equiv 0$ was taken with the low-frequency filter $\hat{w}_1$ of (3.5). Further iterative reconstruction mentioned in section 2 very little improves the result given by f_2 for the examples of the present note. For the examples of the present note, we consider the product $\lambda_1\lambda_2$ as a number meaning the part of g^- that is out of the range of $P_{\tilde{a}}$.

Reconstruction results on Ξ_2, Ξ_3 shown in figures 6 and 7 are not yet perfect because in this note our algorithm properly corrects only for nonuniform attenuation effects (among all the physical effects arising in SPECT). Reconstruction results on Ξ_2, Ξ_3 look better if we reduce the parameter β from $1/2$ to $1/4$. This reconstruction result on Ξ_3 is shown in figure 8.

Finally, figure 9 shows the image reconstructed on Ξ_3 via (1.2) with $a \equiv 0$, where H was taken with the low-frequency filter $\hat{w}_1$ of (3.5), figure 10 shows the image reconstructed on Ξ_3

by the initial algorithm of [Ku], where H in (1.2c) was taken with the low-frequency filter $\hat{w}_1$ of (3.5).

The reconstruction shown in figure 9 is stable but contains the usual errors of no attenuation correction (for example, a considerable negative artifact in the region (E) (defined in figure 1)). In fact, negative artifacts make a great contrast between the regions (E), (D) on one hand, and region (B) on the other hand, as seen in figure 9. However, these artifacts could mask the emission activity in (E) and (D) in some other cases of the radionuclide distribution.

The reconstruction shown in figure 10 is still rather unstable.

4. Conclusions

The noise sensitivity of the initial algorithm of [Ku] implementing numerically the inversion formula (1.2) is significantly reduced by means of the techniques described in section 2.

The results of the present note show that the formula (1.2) can indeed be used for nonuniform attenuation correction in real SPECT imaging. The formula (1.2) can be used, in particular, for fast computing of an efficient first approximation for more complicated SPECT reconstruction techniques, correcting not only for effects of nonuniform attenuation.

We plan to take further the approach based on (1.2) to nonuniform attenuation correction in SPECT. More precisely, we plan: to study further possibilities to improve the stability of the algorithm based on (1.2), to use this algorithm in the framework of techniques correcting not only for attenuation effects, and to consider further (more interesting) examples of real SPECT imaging.

References

[Ku] Kunyansky L A 2001 A new SPECT reconstruction algorithm based on the Novikov's explicit inversion formula *Inverse Problems* **17** 293–306 (*Preprint* mp-arc/00-342)

[MNOY] Morozumi T, Nakajima M, Ogawa K and Yuta S 1984 Attenuation correction methods using the information of attenuation distribution for single photon emission CT *Med. Imaging Technol.* **2** 20–9

[MIMIKIH] Murase K, Itoh H, Mogami H, Ishine M, Kawamura M, Iio A and Hamamoto K 1987 A comparative study of attenuation correction algorithms in single photon emission computed tomography (SPECT) *Eur. J. Nucl. Med.* **13** 55–62

[Na1] Natterer F 1986 *The Mathematics of Computerized Tomography* (Stuttgart: Teubner)

[Na2] Natterer F 2001 Inversion of the attenuated Radon transform *Inverse Problems* **17** 113–19

[No1] Novikov R G 2002 An inversion formula for the attenuated x-ray transformation *Ark. Mat.* **40** 145–67 (Rapport de Recherche 00/05-3, Université de Nantes, Laboratoire de Mathématiques)

[No2] Novikov R G 2002 On the range characterization for the two-dimensional attenuated x-ray transformation *Inverse Problems* **18** 677–700